A Multimode/Multiband Power Amplifier With a Boosted Supply Modulator

Daehyun Kang, Dongsu Kim, Jinsung Choi, Jooseung Kim, Yunsung Cho, and Bumman Kim, *Fellow, IEEE*

Abstract—A multimode/multiband power amplifier (PA) with a boosted supply modulator is developed for handset applications. A linear broadband class-F amplifier is designed to have a constant fundamental impedance across 1.7–2 GHz and its second and third harmonic impedances are located at the high-efficiency area. To reduce the circuit size for handset application, the harmonic control circuits are merged into the broadband output matching circuit for the fundamental frequency. An envelope-tracking operation delivers high efficiency for the overall power. The linearity is improved by envelope tracking (ET) through intermodulation-distortion sweet-spot tracking at the maximum output power level. The efficiency and bandwidth (BW) are enhanced by a boosted supply modulator. Multimode operation is achieved by an ET technique with a programmable hysteresis control and automatic switching current adaptation of the hybrid supply modulator. For demonstration purpose, the PA and supply modulator are implemented using an InGaP/GaAs heterojunction bipolar transistor and a 65-nm CMOS process. For a long-term evolution signal, the envelope-tracking (ET) PA delivers a power-added efficiency (PAE) and an error vector magnitude of 33.3%–39% and 2.5%–3.5%, respectively, at an average power of 27.8 dBm across 1.7–2 GHz. For a wideband code-division multiple-access signal across 1.7–2 GHz, the ET PA performs a PAE, an ACLR1, and an ACLR2 of 40%–46.3%, from −39 to −42.5 dBc, and −51 to −58 dBc, respectively, at an average output power of 30.1 dBm. The ET PA with an EDGE signal delivers a PAE, an ACPR1, and an ACPR2 of 37%–42%, from −56.5 to −59.3 dBc, and −63.5 to −69.5 dBc, respectively, at an average power of 28 dBm across the 300-MHz BW. These results show that the proposed design achieves highly efficient and linear power amplification for multimode/multiband wireless communication applications.

Index Terms—Efficient, enhanced data rates for GSM evolution (EDGE), envelope tracking (ET), handset, heterojunction bipolar transistors (HBT), linear, long-term evolution (LTE), monolithic microwave integrated circuit (MMIC), power amplifier (PA), supply modulator, wideband code division multiple access (WCDMA).

D. Kang, D. Kim, J. Kim, Y. Cho, and B. Kim are with the Department of Electrical Engineering, Pohang University of Science and Technology (POSTECH), Pohang, Gyeongbuk 790-784, Korea (e-mail: daehkang@postech.ac.kr; bmkim@postech.ac.kr).

J. Choi is with the Samsung Advanced Institute of Technology (SAIT), Yongin-si, Gyeonggi 446-712, Korea.

I. INTRODUCTION

POWER amplifiers (PAs) for multifunctional smart mobile phones have become a very challenging area because the PA should handle voice, data, and broadcast with global roaming capability. Therefore, the PAs should have a multimode/multiband capability with high efficiency [1]. The input/output matching components of the transmitter are sensitive to frequency, thus preventing multiband operation. Low amplification efficiency leads to a short battery life and heat in mobile handsets. Moreover, as the information content increases, modulation systems need to have wider bandwidths (BWs) and a higher peak-to-average power ratio (PAPR), causing the PA to operate in a less efficient back-off region for linearity. To improve the low efficiency at the back-off power region, many efficiency enhancement techniques have undergone research for a long period of time.

The Doherty and the envelope elimination and restoration (EER) techniques have been investigated for high efficiency at the back-off power region. The efficiency at the back-off power region is important for handset applications because of frequent use of lower power levels and the high PAPR of the signals. The Doherty technique modulates the load according to the power level [2]–[5]. The load modulation is often achieved by a quarter-wavelength transformer, and linear operation is accomplished by third-order intermodulation (IM3) cancellation between the main and auxiliary amplifiers. Both of these are sensitive to the frequency of operation. Thus, the Doherty PAs have a limit for broadband operation.

The EER technique involves modulating the supply voltage according to the power level of a PA, and enhances efficiency at the back-off power region [6]–[16]. The EER structure comprises the supply modulator and the PA. Only the PA determines the RF operating frequency band. Thus, the EER technique is more advantageous for broadband operation than the Doherty technique.

The efficiency of the EER structure is determined by multiplication of the efficiencies of the supply modulator and the PA [12]. A highly efficient EER structure requires that both the supply modulator and PA be efficient. Thus, class-E, class-F, class-D, and class-J PAs can be candidates. The class-E PAs achieve high efficiency by turning on the transistor at the point when the drain–source (collector–emitter) capacitor does not have any charge. The class-F PA controls the voltage waveform to ensure it is square shaped, which increases the magnitude of the fundamental voltage, output power, and efficiency [17], [18]. The class-D PA controls the harmonics in a similar way to the

class-F PA, using a push–pull structure. The class-J PA utilizes the phase shift between the output current and voltage waveforms to render the second harmonic termination to a purely reactive regime [19].

The broadband approaches for class-E PAs and class-F PAs have been studied in [20] and [21]. However, these concepts are for base-station PAs, and use microstrip lines for matching. The microstrip lines are too bulky to be employed in PAs for handset applications. In [22], we have proposed broadband class-F PAs, which control the second and third harmonic impedances across a broad BW, but linearity is not considered as we intend to use a digital pre-distortion (DPD) technique. Broadband class-J PAs for base-station PAs have been also investigated [19]. The researchers have found the optimum efficiency contour for class-J operation across a broad BW, and matched the load impedance to the contour, thus, a 50% fractional BW with high efficiency is achieved. A gallium–nitride (GaN) device with a high supply voltage has a low Q for the output impedances due to the small output capacitance, and its gain drops 3 dB per octave frequency (normally it is 6 dB/octave because of its operation at the maximum stable gain (MSG) region). Despite the advantageous characteristics of the GaN device, it is too expensive at the moment to be utilized for handset devices and it requires too high bias voltage.

The ideal EER structure would deliver a 100% efficiency using a highly efficient supply modulator, but the limited BW of switching amplifiers and the low efficiency of wideband linear amplifiers for the modulators degrades the ideal efficiency. Some researchers have utilized the advantages of the wide-BW linear amplifier and the high-efficiency switching amplifier [10]–[15]. The switching amplifier does not follow most of the high slew-rate load current, and operates as a quasi-constant current source. The linear amplifier supplies and sinks the current to regulate the load according to the envelope of the signal. This structure is suitable for the envelope signal of modern wireless communication systems, which has the most power in the low-frequency region. In [15], we have proposed a hybrid switching amplifier (HSA) for multistandard applications. Automatic switching current adaption from an HSA and programmable hysteresis control can achieve multimode operation.

In this paper, we propose a multimode/multiband PA with a boosted supply modulator for handset applications. For this multiband PA design, the fundamental load is maintained at a consistent level across the BW. Harmonic impedances are searched for highly efficient class-F operation. The harmonic circuits are merged into the broadband matching circuit, thereby reducing their size and increasing the available BW. In contrast to our previous paper [22], the PA matching is modified for linear class-AB bias. An HSA with a boost converter driving the linear stage increases the RF BW due to reduced output capacitance of the RF device at the higher operating voltages provided by the boost converter. The HSA also improves the efficiency due to envelope tracking (ET). Finally the HSA improves linearity due to intermodulation-distortion (IMD) sweet-spot tracking. Multimode operation for various wireless applications is accomplished thanks to programmable hysteresis control and automatic switching current adaptation from the HSA.
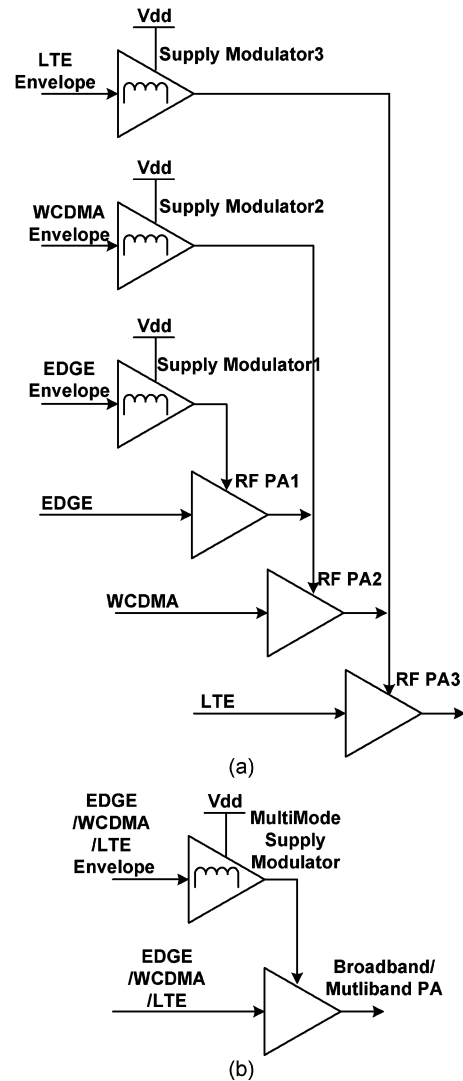

Fig. 1. (a) Conventional polar transmitter for multimode/multiband operation. (b) Proposed polar transmitter for multimode/multiband operation.

For demonstration purposes, the PA and supply modulator are implemented using an InGaP/GaAs HBT and a 65-nm CMOS processes, and are operated with signals of long-term evolution (LTE), wideband code division multiple access (WCDMA), and EDGE across frequencies of 1.7–2 GHz. The measured results prove that the proposed design achieves highly efficient and linear power amplification for multimode/multiband applications.

II. MULTIMODE/MULTIBAND POLAR TRANSMITTER

A conventional polar transmitter for multimode/multiband operation requires a PA and a supply modulator for each wireless communication standard, as shown in Fig. 1(a). For example, if we need transmitters operating for an LTE, a WCDMA, and an EDGE application across a 1.7–2.0-GHz frequency, supply modulators and PAs need to operate at different switching frequencies and operate at different RF frequencies for each standard. The LTE signal has a BW of 10 MHz and a PAPR of 7.5 dB. WCDMA and EDGE signals have BWs of

3.84 MHz and 384 kHz, respectively, and a PAPR of 3.5 dB. Each supply modulator for each application should be employed for multimode operation. Moreover, if a narrowband PA is used, then every RF band will require the addition of another PA.

Therefore, for simplicity and low cost, we propose a multimode/multiband ET polar transmitter using a multimode supply modulator [15] and a broadband class-F PA [22], as illustrated in Fig. 1(b). The broadband class-F PA can cover the frequency band of 1.7–2 GHz while maintaining high efficiency and linearity. This will be revisited in Sections III and IV. The switching frequency and switching currents of the switching stage can be controlled by programmable hysteresis control and automatic switching current adaptation from the hybrid supply modulator according to each communication application. Moreover, by employing the ET technique, the supply voltage provided to the PA follows the envelope of the signal so the dc power that the PA consumes can be significantly reduced, and the power-added efficiency (PAE) can be significantly increased at the average power level, as well as at the peak output power level.

III. TECHNIQUES FOR HIGH EFFICIENCY AND BROADBAND

A. Class-AB/F PAs

A highly efficient class-AB/F PA has been proposed in [25], which enhances the efficiency by controlling the second and third harmonics while maintaining their linearity. By setting the base bias to near class B, it efficiently amplifies phase-only information such as the global system for mobile communications (GSM) signal. With a bias level of class AB, it efficiently and linearly amplifies both the phase and amplitude information including CDMA, LTE, WiMAX, and EDGE signals. The output load impedance R_{opt} is set to an intermediate value for multimode operation. Class-E, inverse class-F, or class-J PAs can provide an even higher efficiency or a broader BW, but we adopt the efficient and linear class-F PA for ET operation because linearity improvement techniques such as DPD are still a burden for the PAs of handset applications.

To employ a class-AB/F PA for an ET polar transmitter with a boosted supply voltage ($V_{cc} = 4.5$ V), the fundamental load impedance is set to be $6 + j1\ \Omega$ for a 1-dB compression power (P1 dB) of 32 dBm, and a class-AB bias level (98 mA) is chosen. The second and third harmonic impedances are found for high-efficiency operation with a fixed fundamental output load, as shown in Fig. 2. This figure shows that a third harmonic impedance several times larger than the fundamental load impedance delivers high efficiency. This can be easily achieved across the broadband frequency range. The second harmonic impedance is more sensitive to the matching circuit than the third harmonic impedance, but is manageable over a few hundred megahertz BW using a second harmonic control circuit.

B. Broadband Matching Techniques

There are equations that transform a low-pass filter (LPF) to a bandpass filter (BPF) [26]. The BPF does not allow the impedance transformation required for PA designs. The BPFs
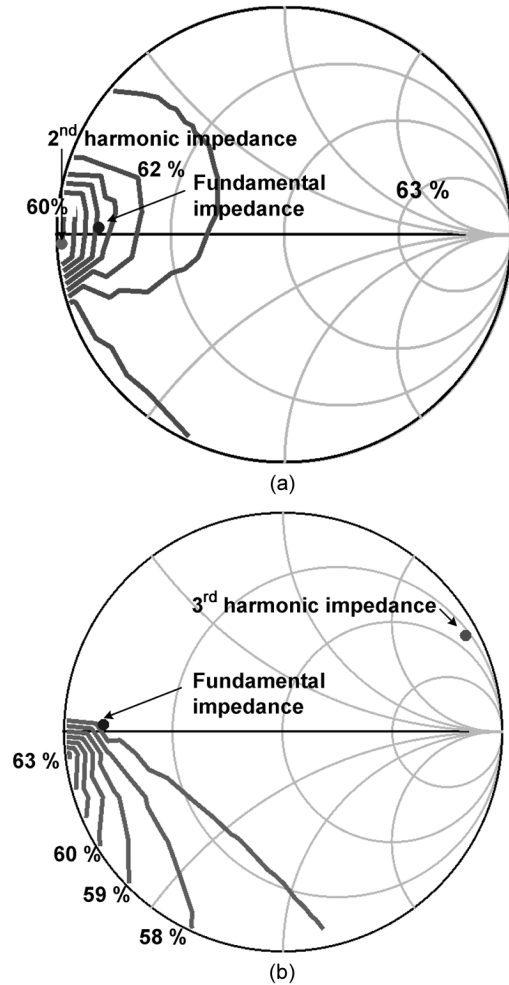

(a)

(b)

Fig. 2. Simulated load–pull results at a frequency of 1.85 GHz. (a) For third harmonic impedance. The fundamental and second harmonic impedances are fixed at $6 + j1$ and $0.5 - j2.5$, respectively. (b) For second harmonic impedance. The fundamental and second harmonic impedances are fixed at $6 + j1$ and $25 + j200$, respectively.

shown in Fig. 3(c) and (d) make it possible to transform the impedances and to have bandpass characteristics. To analyze the BW, the concept of Q needs to be recalled. A loaded Q, denoted by Q_L, is defined by

$$Q_L = \frac{Q_n}{2} = \frac{f_o}{\mathrm{BW}}. \qquad (1)$$

The circuit node Q, denoted by Q_n, is defined at each node as

$$Q_n = \frac{|X|}{R} = \sqrt{\frac{R_T}{R_S} - 1} \qquad (2)$$

where R_T is a transformed resistance from R_S and R_T is larger than R_S. The smaller Q_n leads to broader BW, which means that the same impedance transformation ratio using two-section matching achieves a wider BW. In Fig. 3(c)–(f), to get the lowest Q_n with the impedance transformation, the relationship of impedances is given by

$$R_2 = \sqrt{R_1 \cdot R_3}. \qquad (3)$$

Fig. 3(e) is a high-pass filter (HPF) type matching circuit, which comprises two sections, and it has the same Q as
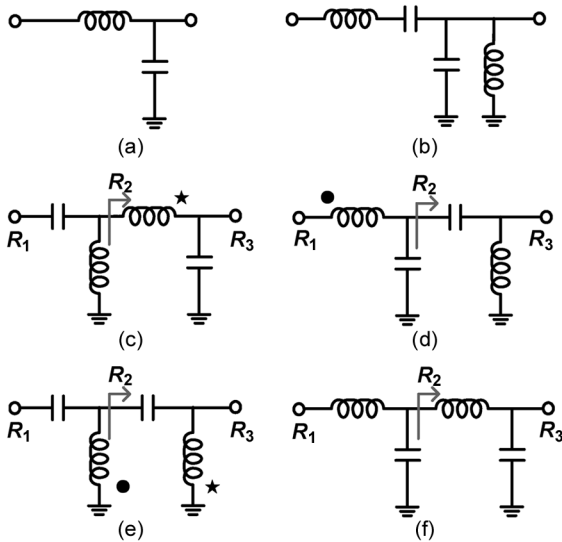
Fig. 3. Impedance-matching circuits. (a) LPF type. (b) BPF type. (c) and (d) BPF type with impedance transformation. (e) Two-section HPF type. (f) Two-section LPF type.

Fig. 3(c) and (d). The 3-dB BW might be the same, but the BPF types are better because the BPFs maintain more consistent impedance level across lower to upper bands. Moreover, the BPF types shown in Fig. 3(c) and (d) have an advantage of smaller inductance than the HPF of Fig. 3(e) because a series inductance (reactance) is smaller than a shunt inductance (susceptance) where a low impedance is transformed into a high impedance of 50 Ω in the PA designs. The series inductors marked with a star and with a circle in Fig. 3(c) and (d), respectively, are smaller than those marked in Fig. 3(e). Fig. 3(f) is an LPF type matching circuit. Even though the BW is broad, an LPF is a unwelcome circuit for the input and output matching of handset PAs because dc currents from the supplies should be blocked. The BPFs shown in Fig. 3(d) are employed in this broadband class-F PA design because of their broadband characteristics and their small inductor values, which can be easily replaced by bondwires.

C. Input, Interstage, and Output Matching

As illustrated in Fig. 4, an input capacitance composed of C_{be} and C_{bc} increased by Miller's theorem is merged into the series inductor of the LC–CL broadband matching circuit [see Fig. 3(d)] to maximize the BW. The intermediate impedance is set as 10 Ω to transform the 2 Ω of the input resistance to the 50 Ω of the input terminal. The interstage is matched with two-section HPFs, including the bias line inductance at the collector of the drive stage. The HPFs also have a low-impedance transformation ratio to maximize the BW. The output matching comprises a broadband fundamental impedance matching, the second harmonic short circuits and the third harmonic open circuit. L_2C_2 has a near zero impedance at the upper band of the second harmonic and C_{22} with a short microstrip line has a near-zero impedance at the lower band of the second harmonic. Thus, the voltage waveform of the second harmonic is effectively reduced across the broadband. The shunt L_3C_3 provides a high impedance at the third harmonic frequency. The output

capacitance C_p is resonated out at the third harmonic frequency by the inductance at the bias line. The fundamental impedance matching uses LC–CL type broadband matching. The shunt L_3C_3 has an inductance at the operating frequency, and can be merged into a bondwire L_1 for broadband matching.

The simulated load impedances including the components' loss are shown in Fig. 5(a). The load impedances across the 1.7–2.0-GHz frequency are constant with power matching. The second harmonic impedances across the 3.4–4.0-GHz frequency are near zero, which is located at the high-efficiency region in Fig. 2(b). The third harmonic impedances across the 5.1–6.0-GHz frequency are high, which is also located at the high efficiency region in Fig. 2(a).

Fig. 5(b) shows the broadband characteristic of the insertion loss $S21$ over the frequency rage of 1.7–2.0 GHz. $S21$ has the two nulls at 3.3 and 3.8 GHz, which are produced by C_{22} with a short microstrip line and L_2C_2, respectively. With this circuit topology, the harmonic control circuits are merged into the fundamental matching elements, realizing a small size for handset applications.

D. Boosted Supply Voltage

The supply voltage of the linear stage of the HSA is increased from 3.4 to 5 V by the boost converter depicted in Fig. 4. Since the buffer comprising the linear stage has a voltage drop of 0.5 V, the output voltage swing of the supply modulator is boosted up to 4.5 V. Our previous HSA [15] had a maximum output voltage of only 3 V. Due to the boosted output voltage, the PA can generate more power with the same output load. In other words, the output load impedance can be raised for the same output power as illustrated in Fig. 6, which delivers a higher efficiency and broadband characteristics. The broadband characteristics are explored using the output capacitance variation plot shown in Fig. 7. The supply voltage V_{cc} is swept with fundamental load impedances of 2.5, 3.5, 4.7, and 6 Ω, which deliver the same output power with the maximum supply voltages of 3, 3.5, 4, and 4.5 V, respectively. When ET operation follows the highest efficiency at each supply voltage, the output capacitance of the transistor follows the C_{out} trajectory in Fig. 7. The output capacitance is calculated by the method shown in [24]. As the supply voltage decreases, the output capacitance increases. At an output power of 32 dBm, the PA using R_{opt} of 2.5 Ω with a supply voltage of 3 V has about a 10% larger output capacitance than that using R_{opt} of 6 Ω with a supply voltage of 4.5 V. If an LTE signal with a 7.5-dB PAPR is applied to the PA, the maximum average power is theoretically 24.5 dBm because the P1 dB of the PA is 32 dBm. In actual operation, however, the PA can achieve an average output power of about 28 dBm because some portion of the peak signal could be saturated while maintaining an acceptable linearity specification. Besides the smaller output capacitance, the PA with a 4.5-V V_{cc} has a smaller impedance transformation ratio, which assists in increasing the operational RF BW. Fig. 8(a) shows a simulated continuous wave (CW) performance for PAE and gain of the supply voltages of 2.6 V with a load of 6 Ω and 2 V with a load of 2.5 Ω for the power stage. The supply voltages are reduced for operation of the LTE average output power of 28 dBm. The PA with 6 Ω has 10% higher PAE and higher gain. Fig. 8(b) shows the insertion loss obtained by a
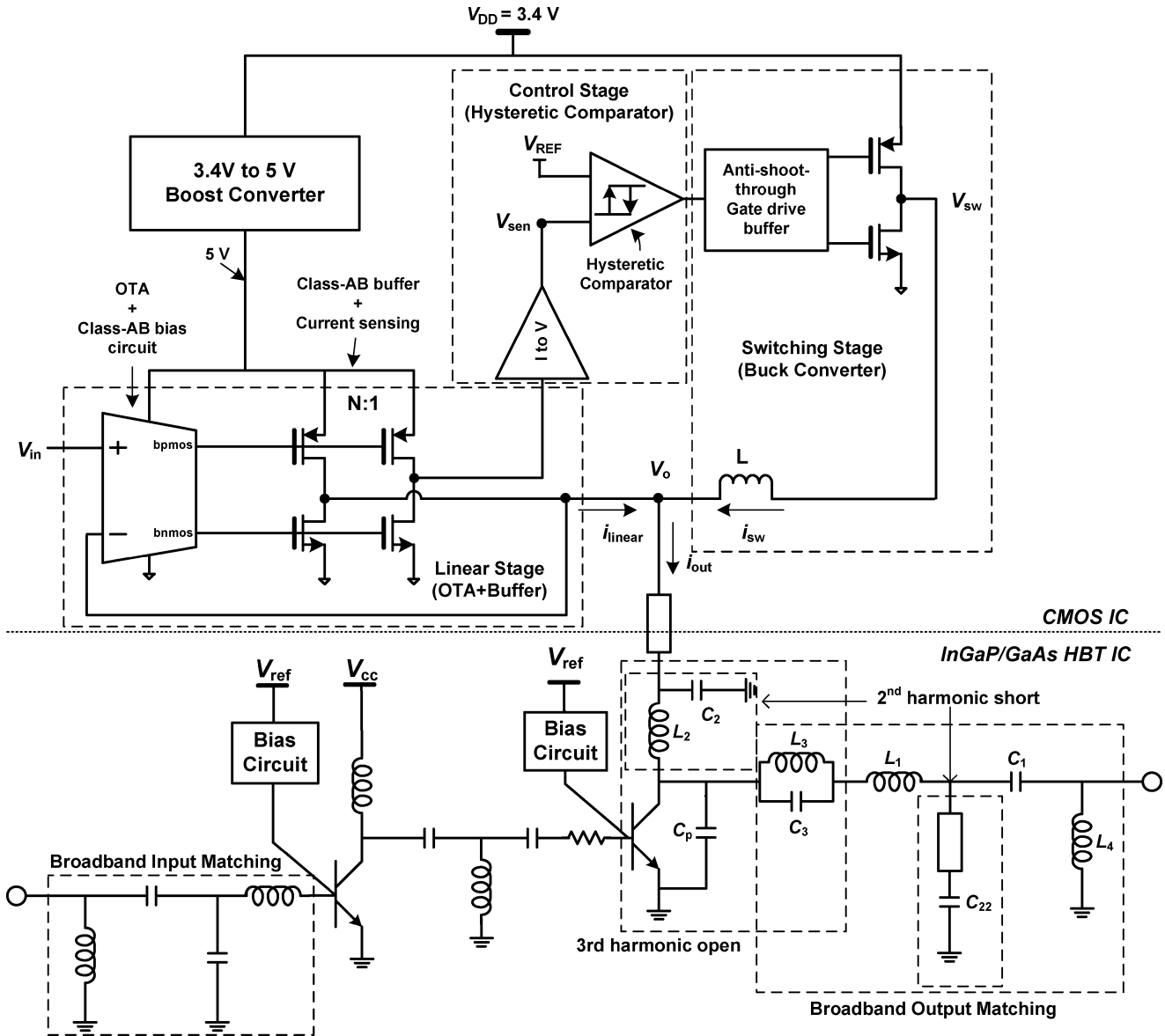
Fig. 4.   Schematic of the ET transmitter with broadband class-F PA and boosted supply modulator.

large-signal S-parameter at an output power of 28 dBm, which shows a broader BW for a supply voltage of 2.6 V because of the smaller output capacitance and the impedance transformation ratio.

## IV. TECHNIQUES FOR MULTIMODE OPERATION OF HSA

An HSA consists of a boost converter, linear stage, hysteretic comparator, and switching stage, as shown in Fig. 4. The boost converter is connected to the linear stage to boost the output voltage swing. The linear stage works as an independent voltage source throughout the feedback network, while the switching stage operates as a dependent current source to provide most of the current to the output. The current sensing circuit detects the current at the output of the linear stage, and controls the state of the switching stage according to the magnitude and polarity of the sensed current. A detailed overview of the HSA operation is explained clearly in [15]. Multistandard signals have different

PAPRs and BW. The adaptation of the switching currents for the various PAPRs are automatically performed by the current sensing circuit and the hysteretic comparator in the HSA. The switching current is proportional to the difference between V_{sen} and V_{REF}, as shown in Fig. 4. The sensed current generates the sensed voltage V_{sen}, which is proportional to the input of the envelope signal. Thus, the square of the switching current is inversely proportional to the PAPR.

The adaptation of switching currents for multistandard signals is shown in Fig. 9, which illustrates the probability density function (pdf) and the efficiency of the HSA. For a multimode HSA design, the switching condition is optimized for the wideband signal by determining an inductor value at the output of the switching stage. A narrowband signal whose slew rate is lower than that of the switching amplifier leads to an excessively high switching frequency and poor efficiency of the switching stage. Thus, we utilize a programmable hysteretic comparator, which enables us to control the hysteresis voltage V_{hys}, and the
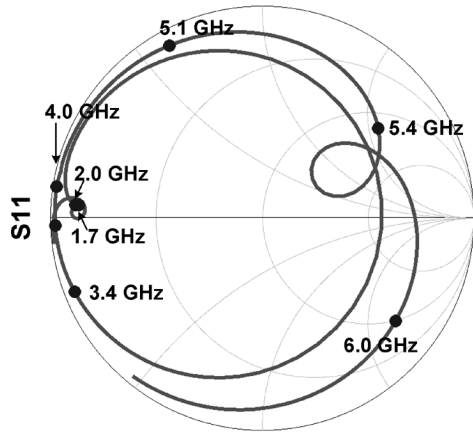
(a)
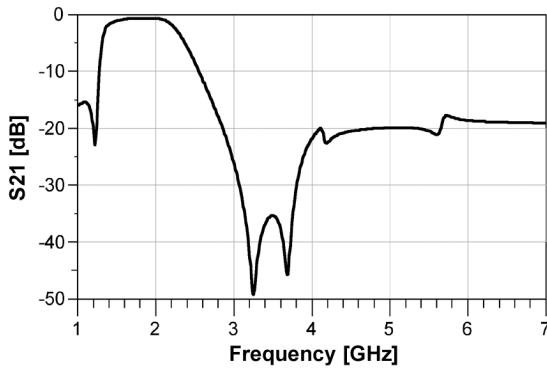
(b)

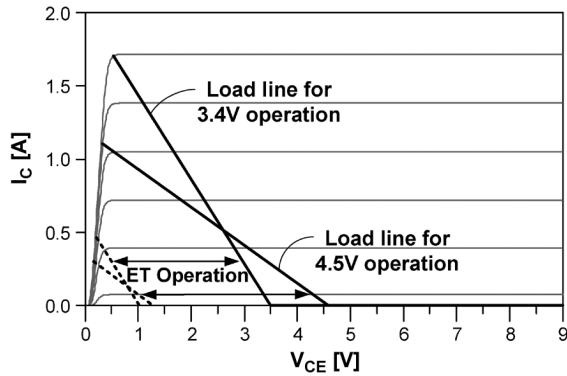Fig. 5. Simulated S-parameters of output matching circuit including components' loss.

Fig. 6. Load line of 2.5 and 6 Ω for 3.4- and 4.5-V operation for the same maximum output power. Load line for 4.5 V gives higher efficiency and broader BW, as well as more linear ET operation at the low-power level.

Fig. 7. Output capacitance as functions of R_{opt}, V_{cc}, and output power. With an ET operation, the output capacitance of the PA follows the C_{out} trajectory.

(a)

(b)

Fig. 8. (a) Simulated CW performance of PAE and gain with supply voltages of 2.6 and 2 V for the power stage. The PAs with 2.6- and 2-V V_{cc} have R_{opt} of 6 and 2.5 Ω, respectively, to generate the same powers. Ideal LC–CL type broadband matching circuits are employed at the input and the output. (b) Simulated large-signal insertion loss at an output power of 28 dBm.

switching frequency. Efficiency of about 3% is enhanced by controlling the hysteresis voltage for the EDGE signal.

The envelope is modified for linear ET operation, as depicted in Fig. 10. The equation for the envelope shaping is given by

$$\mathrm{Envelope}' = \left(1 - \frac{V_{\mathrm{knee}}}{V_{\mathrm{peak}}} \cdot 10^{x/20}\right) \cdot \mathrm{Envelope} + \mathrm{Offset} \quad (4)$$

where x is a back-off power level from the peak average power. The PA has AM/AM and AM/PM distortions at a low supply voltage because of the increased output capacitance, as shown
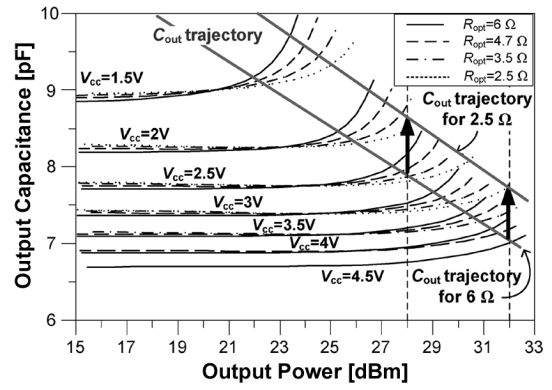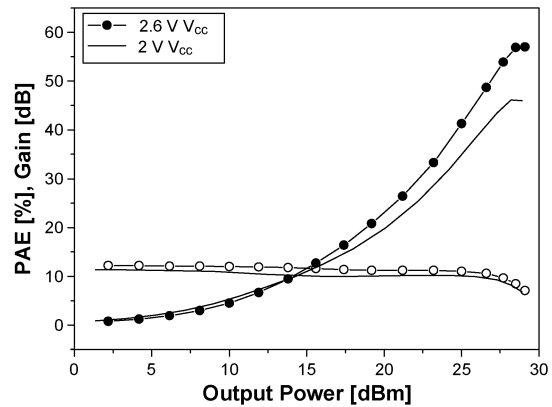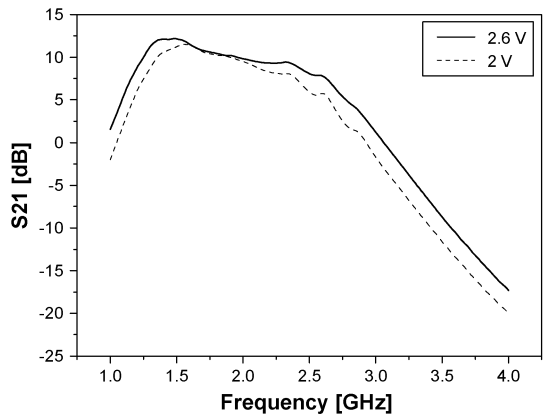
in Fig. 7, and increased ratio of knee to the V_{CC}. Thus, the minimum of the envelope is set as 0.8 V. As the power level is varied, the slope of the envelope is modified by the equation for the compensation of low gain near the knee region while maintaining the offset voltage. It is noted that x (back-off) = -1 or a lower value is applied to the equation for the maximum average output power because PAs often operate in saturation, but is still under the specification. With the envelope-shaping method, the PA always operates at the IMD sweet spot tracked
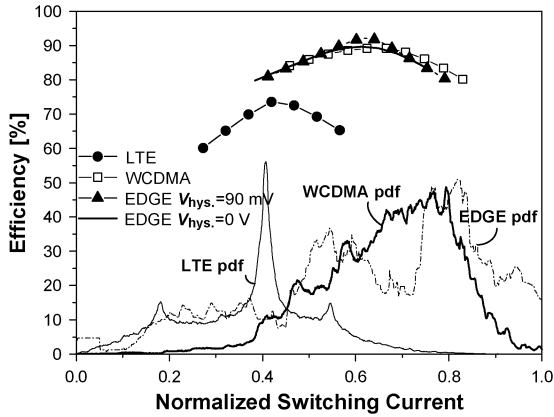
Fig. 9. Simulated average switching currents adaptation for LTE, WCDMA, and EDGE signals. The switching currents are normalized as 640 mA. The pdf of each signal is also depicted as a function of $\overline{i_{sw}}(= V_{out}/R_{load})$.
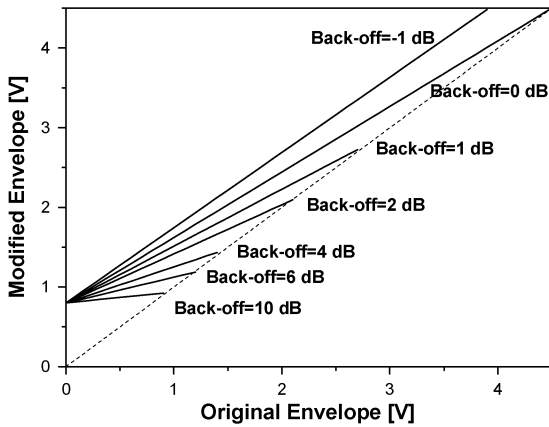

Fig. 10. Function of envelope shaping.

Fig. 11. Measured and simulated S-parameters with a supply voltage of 3.4 V.
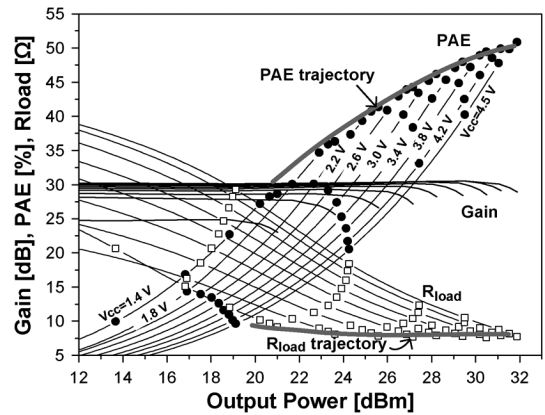
Fig. 12. Measured CW performance at 1.85 GHz by sweeping a collector voltage from 1.4 to 4.5 V.

by the envelope of signal, and the overall IMD level is lowered significantly [23].

V. EXPERIMENTAL RESULTS

The proposed multimode/multiband PA with a boosted supply modulator is fabricated in an InGaP/GaAs HBT 2-μm process and a CMOS 65-nm process, respectively. The HBT PA is integrated onto a chip, except for five capacitors at the input and the output. Inductors are replaced by bondwires and slab inductors on the chip to ensure low loss. The second harmonic control circuit is implemented with an off-chip capacitor and a bonding wire, and the third harmonic control is accomplished by on-chip slab inductors and metal–insulator–metal (MIM) capacitors for a high-Q factor. For the CMOS supply modulator, all the circuit blocks are integrated on the chip, except the large inductor. The two chips are mounted on an FR-4 printed circuit board. The broadband PA is built by comparing the simulated and measured S-parameter results. Fig. 11 shows that the simulated and measured results with a supply voltage of 3.4 V are well matched and $S21$ shows a flat response across the fundamental frequencies (1.7–2 GHz). The quiescent currents are set as 38 and 98 mA for the drive and power stages, respectively. It is interesting to note that with the supply modulator, the 98-mA quiescent current is reduced as the input power decreases, and it becomes 3 mA when
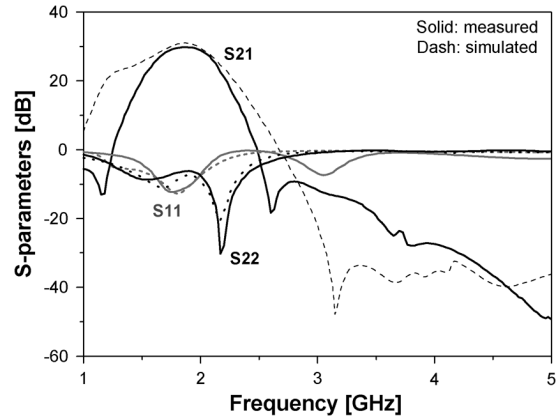
there is no input signal that turns off the switching stage and outputs 0.5 V from the linear stage of the supply modulator. The fabricated PA with a supply voltage of 4.5 V delivers a P1 dB of 31.5 dBm, a gain of 29.5 dB, and a PAE of 49.8% at a frequency of 1.85 GHz, as shown in Fig. 12. The supply voltage is swept from 1.4 to 4.5 V, and the expected PAE for the ET operation follows the measured PAE trajectory. The measured performance of the HSA is summarized in Table I. The supply modulator has a peak efficiency of 90% for a load impedance of 8 Ω, and delivers an output swing of 0.5–4.5 V thanks to the boost converter connected to the linear stage. The switching frequency for an EDGE signal is reduced to 3.4 MHz from the switching frequency of 10.5 MHz (at $V_{hys.} = 0$) by increasing $V_{hys.}$ to 90 mV because the low switching provides a higher efficiency for the EDGE signal, which has a low slew rate due to the narrow BW (384 kHz). The average switching currents are adjusted for the signals' pdf.

For a demonstration of multimode/multiband operation, the ET PA is tested with 10-MHz BW 16 quadrature amplitude modulation (16-QAM) 7.5-dB PAPR LTE, 3.84-MHz BW 3.5-dB PAPR WCDMA, and 384-kHz BW 3.5-dB PAPR EDGE signals. Fig. 13(a) shows the measured performance of the ET PA across a 1.7–2-GHz frequency for the LTE signal. The PA has a PAE and an error vector magnitude (EVM) of 33.3%–39% and 2.5%–3.5%, respectively, at the average

TABLE I
PERFORMANCE OF THE MULTIMODE SUPPLY MODULATOR

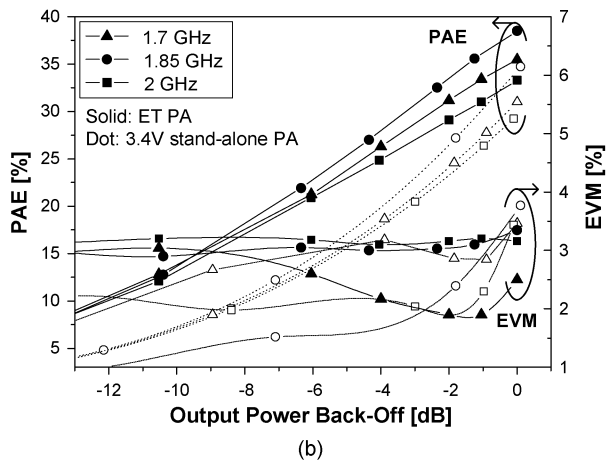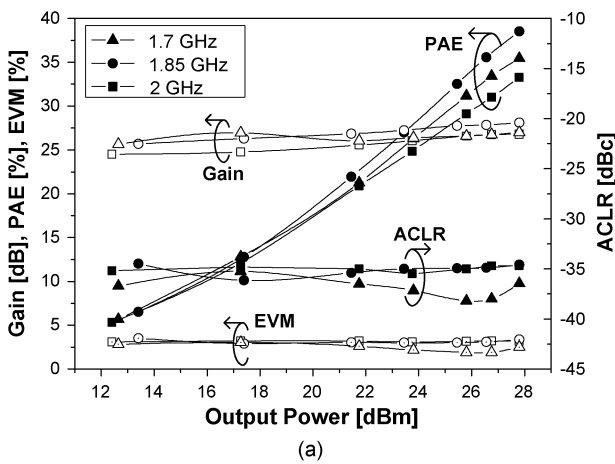| Parameters	Values
Supply Voltage	3.3 V
Output voltage range	0.5-4.5 V
Output RMS current	0-700 mA
Peak efficiency	90%
Minimum GBW	100 MHz
f_{sw} (at $V_{hys.}$) for EDGE	3.4 MHz (90 mV)
for WCDMA	1.6 MHz (0 V)
for LTE	7.1 MHz (0 V)
$\overline{i_{sw}}$ at the maximum power for EDGE	400 mA
for WCDMA	400 mA
for LTE	270 mA

Fig. 13. (a) Measured performance of ET PA across 1.7–2 GHz for a 10-MHz BW 16-QAM 7.5-dB PAPR LTE signal. (b) Measured performance comparison of ET PA and standalone PA, and the maximum output powers are 27.8 and 25.9 dBm, respectively.
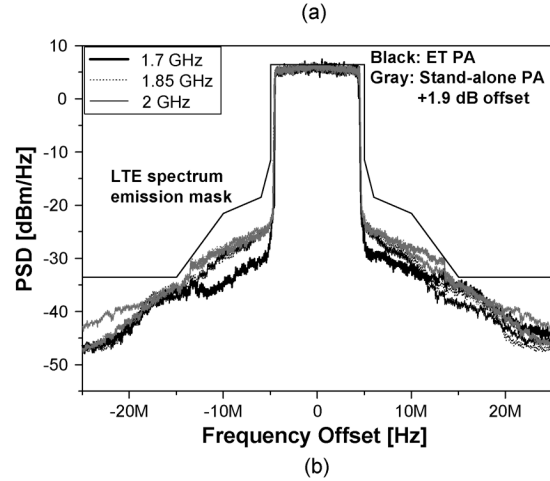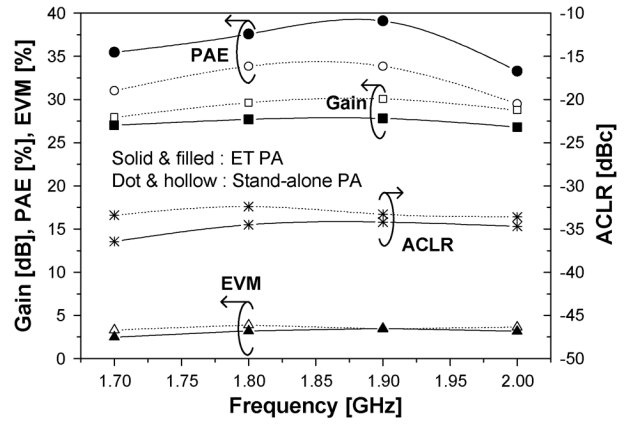

Fig. 14. (a) Measured performance of ET PA and standalone PA at the output powers of 27.8 and 25.9 dBm, respectively, across 1.7–2 GHz. (b) Measured spectra.

output power of 27.8 dBm. The gain is 26.8–27.8 dB across the BW. ACLR is measured with a 9-MHz resolution BW at both a center frequency and a 10-MHz offset. The ACLR is shown below the LTE ACLR specification of −30 dBc.

Fig. 13(b) shows the performance comparison of the ET PA with the boosted supply modulator and the standalone PA with a supply voltage of 3.4 V. The output power is 27.8 dBm for the ET PA and is 25.9 dBm for the standalone PA. The boosted

supply modulator provides the ET PA a dc voltage swing from 0.5 to 4.5 V so larger output power is generated from the ET PA than the standalone PA with a 3.4-V supply voltage with the same R_{opt}. The PAE is improved by more than 4% at the peak average power across the BW, and the PAE is enhanced by up to 7% at the back-off power region. It is worthwhile to note that the linearity of the ET PA is improved at the peak average power level due to the IMD sweet-spot tracking that we proposed in [23].

Fig. 14(a) shows the measured performance of the ET and standalone PAs at power levels of 27.8 and 25.9 dBm, respectively, across the 1.7–2-GHz frequency. It is noted that the gain performance for the ET operation is flatter across the 1.7–2-GHz frequency because of the relatively smaller output capacitance, thanks to the boosted supply modulator. The EVM and ACLR, which indicate the linearity of the PA, are improved by ET operation.

Fig. 14(b) is the spectra of the ET PA and the standalone PA at power levels of 27.8 and 25.9 dBm. The ET PA has more margin under the LTE spectrum mask. Fig. 15 is a comparison of measured EVM, and the EVM performance is improved from 3.4% to 2.5% at a frequency of 1.7 GHz due to the sweet-spot tracking [23].

Fig. 16 shows the performance comparison of the ET PA with the boosted supply modulator and the standalone PA with
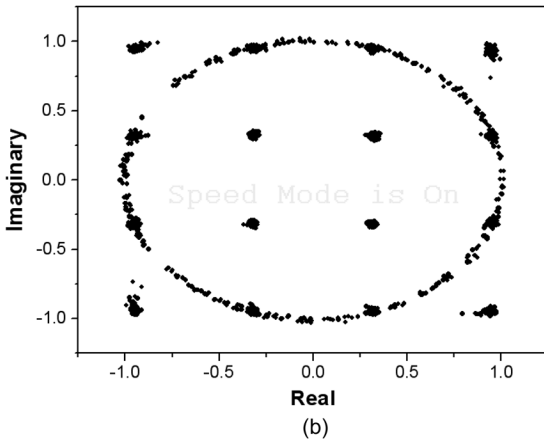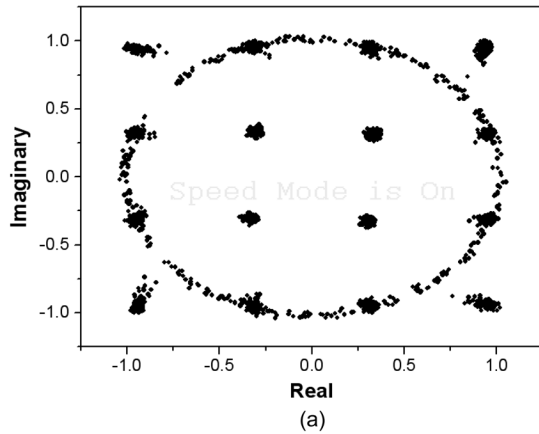
Fig. 15. Measured EVM at a frequency of 1.7 GHz. (a) 3.4% EVM at an average power of 25.9 dBm for the 3.4-V standalone PA. (b) 2.5% EVM at an average power of 27.8 dBm for the ET PA with the boosted supply modulator.

Fig. 16. Measured performance of ET PA and standalone PA for a 3.84-MHz BW 3.5-dB PAPR WCDMA signal across 1.7–2 GHz, and the maximum output powers are 30.1 and 28.1 dBm, respectively.

a supply voltage of 3.4 V for a WCDMA signal, which has a BW of 3.84 MHz and a PAPR of 3.5 dB. In comparison with Fig. 13(b), the PAE for the WCDMA signal at the peak average output power shows 1%–2% less improvement than that for the LTE due to the lower PAPR of WCDMA, and the ACLR at the peak average power shows more improvement because the linear stage of the supply modulator has less of a BW burden for the 3.84-MHz WCDMA signal. At a back-off average output
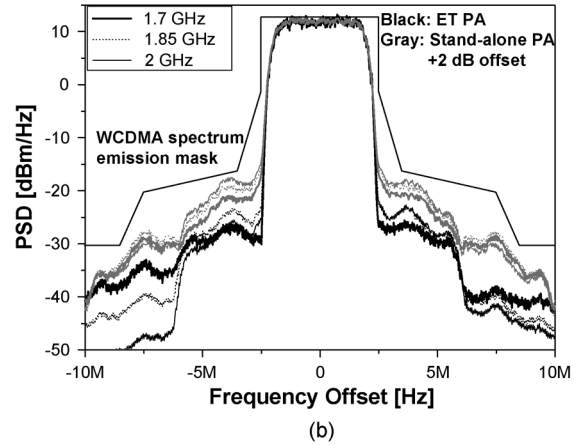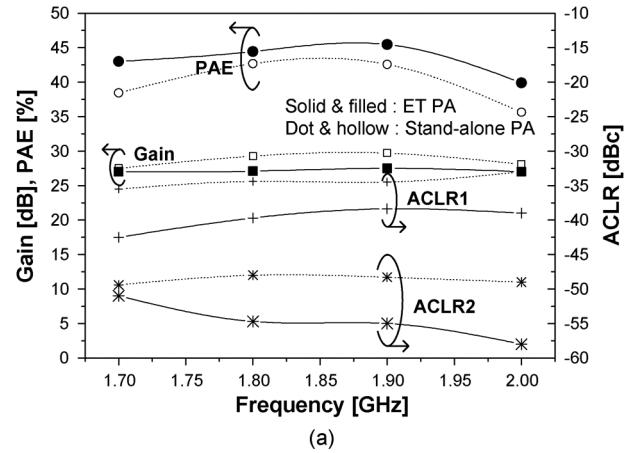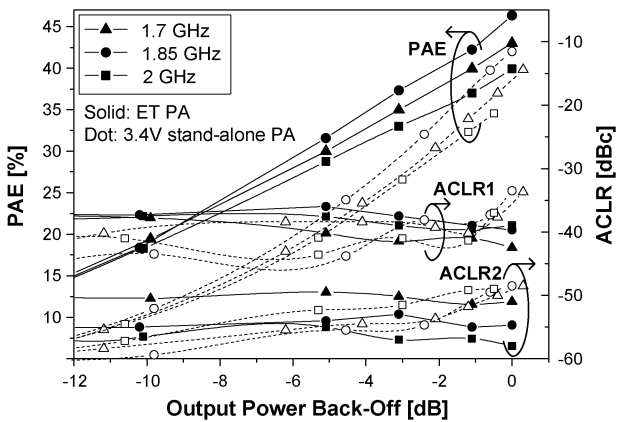

Fig. 17. (a) Measured performance of ET PA and standalone PA for a WCDMA signal at the output powers of 30.1 and 28.1 dBm, respectively, across 1.7–2 GHz. (b) Measured spectra.

power region (∼8 dB), the PAE for the WCDMA has a greater improvement because of the higher efficiency of the supply modulator due to the lower PAPR than that for the LTE signal.

ACLR1 and ACLR2 are measured with a 3.84-MHz resolution BW at frequency offsets of 5 and 10 MHz, respectively. ACLR1 and ACLR2 are measured below the WCDMA ACLR specification of −33 and −43 dBc, respectively, for the ET PA.

Fig. 17(a) shows the measured performance of the ET PA and standalone PA at the output powers of 30.1 and 28.1 dBm, respectively, across a 1.7–2-GHz frequency.

Fig. 17(b) shows the measured spectra of the ET PA and the standalone PA at the output powers of 30.1 and 28.1 dBm, respectively.

The ET PA is also performed with an EDGE signal, which has the BW of 384 kHz and the PAPR of 3.5 dB. Fig. 18(a) shows the performance of the ET PA and the standalone PA with a supply voltage of 3.4 V at the average output powers of 28 and 27 dBm, respectively. The PAE of the ET PA is improved by 3%–4% than that of the standalone PA. ACPR1 and ACPR2 are measured with a 30-kHz BW at frequency offset of 400 and 600 kHz. The hysteresis voltage $V_{hys.}$ is set to 90 mV to reduce the switching frequency f_{sw}, from 10.7 to 3.4 MHz. The overall PAE is then improved by about 2%.

Fig. 18(b) shows the measured spectra. The ACPR around the offset frequency of 400 kHz is improved and the ACPR at the
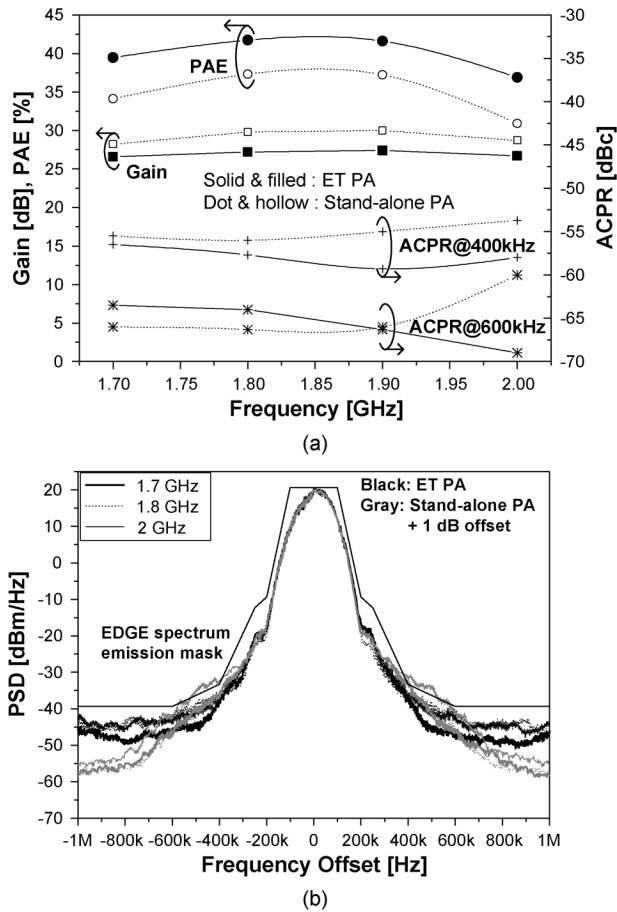
Fig. 18. (a) Measured performance of ET PA and standalone PA for an EDGE signal at the output powers of 28 and 27 dBm, respectively, across 1.7–2 GHz. $V_{hys.}$ is set to be 90 mV for f_{sw} of 3.4 MHz. (b) Measured spectra.

outband is degraded because the ripple currents increase as the switching frequency decreases, but the spectrum is still under the EDGE specification of −60 dBc.

VI. CONCLUSIONS

A multimode/multiband PA with a boosted supply modulator is developed for handset applications. A linear broadband class-F amplifier is designed to operate across a 1.7–2-GHz frequency. The harmonic control circuits are merged into the broadband output matching circuit for the fundamental frequency. The efficiency and BW are enhanced by the boosted supply modulator. The ET operation delivers high efficiency at the overall power level and improves the linearity at the maximum output power by IMD sweet-spot tracking. Multimode operation for various wireless application is accomplished thanks to programmable hysteresis control and automatic switching current adaptation from the HSA. For an LTE signal, the ET PA delivers a PAE and an EVM of 33.3%–39% and 2.5%–3.5%, respectively, at an average output power of 27.8 dBm across 1.7–2 GHz. For a WCDMA signal across 1.7–2 GHz, the ET PA performs a PAE, an ACLR1, and an ACLR2 of 40%–46.3% from −39 to − 42.5 dBc, and −51 to − 58 dBc, respectively, at an average output power of 30.1 dBm. The ET PA with an EDGE signal delivers a PAE, an ACPR1, and an ACPR2 of 37%–42%, from

−56.5 to − 59.3 dBc, and −63.5 to − 69.5 dBc, respectively, at an average output power of 28 dBm. These results verify that the proposed design achieves highly efficient and linear power amplification for multimode/multiband wireless communication applications.
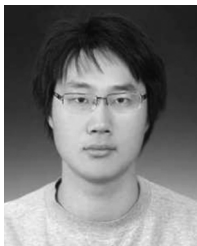
REFERENCES

[1] S. C. Cripps, *Advanced Techniques in RF Power Amplifier Design*. Norwood, MA: Artech House, 2002.
[2] W. H. Doherty, "A new high efficiency power amplifier for modulated waves," *Proc. IRE*, vol. 24, no. 9, pp. 1163–1182, Sep. 1936.
[3] F. H. Raab, "Efficiency of Doherty RF power amplifier systems," *IEEE Trans. Broadcast.*, vol. BC-33, no. 3, pp. 77–83, Sep. 1987.
[4] M. Iwamoto, A. Williams, P. F. Chen, A. G. Metzger, L. E. Larson, and P. M. Asbeck, "An extended Doherty amplifier with high efficiency over a wide power range," *IEEE Trans. Microw. Theory Tech.*, vol. 49, no. 12, pp. 2472–2479, Dec. 2001.
[5] D. Kang, J. Choi, D. Kim, and B. Kim, "Design of Doherty power amplifiers for handset applications," *IEEE Trans. Microw. Theory Tech.*, vol. 58, no. 8, pp. 2134–2142, Aug. 2010.
[6] L. Kahn, "Single-sideband transmission by envelope elimination and restoration," *Proc. IRE*, vol. 40, no. 7, pp. 803–806, Jul. 1952.
[7] D. K. Su and W. J. McFarland, "An IC for linearizing RF power amplifiers using envelope elimination and restoration," *IEEE J. Solid-State Circuits*, vol. 33, no. 12, pp. 2252–2258, Dec. 1998.
[8] J. Staudinger, B. Gilsdorf, D. Newman, G. Norris, G. Sadowniczak, R. Sherman, and T. Quach, "High efficiency CDMA power amplifier using dynamic envelope tracking technique," in *IEEE MTT-S Int. Microw. Symp. Dig.*, Jun. 2000, pp. 873–976.
[9] P. Raynaert and S. Steyaert, "A 1.75-GHz polar modulated CMOS RF power amplifier for GSM-EDGE," *IEEE J. Solid-State Circuits*, vol. 40, no. 12, pp. 2598–2608, Dec. 2005.
[10] J. Kitchen, W. Chu, I. Deligoz, S. Kiaei, and B. Bakkaloglu, "Combined linear and Δ-modulated switched-mode PA supply modulator for polar transmitters," in *IEEE Int. Solid-State Circuits Conf. Tech. Dig.*, Feb. 2007, pp. 82–83.
[11] T. Kwak, M. Lee, B. Choi, H. Le, and G. Cho, "A 2 W CMOS hybrid switching amplitude modulator for EDGE polar transmitter," in *IEEE Int. Solid-State Circuits Conf. Tech. Dig.*, Feb. 2008, pp. 518–519.
[12] F. Wang, D. F. Kimball, J. D. Popp, A. H. Yang, D. Y. C. Lie, P. M. Asbeck, and L. E. Larson, "An improved power-added efficiency 19-dBm hybrid envelope elimination and restoration power amplifier for 802.11g WLAN applications," *IEEE Trans. Microw. Theory Tech*, vol. 54, no. 12, pp. 4086–4099, Dec. 2006.
[13] F. Wang, D. F. Kimball, D. Y. Lie, P. M. Asbeck, and L. E. Larson, "A monolithic high-efficiency 2.4-GHz 20-dBm SiGe BiCMOS envelope-tracking OFDM power amplifier," *IEEE J. Solid-State Circuits*, vol. 42, no. 6, pp. 1271–1281, Jun. 2007.
[14] W. Chu, B. Bakkaloglu, and S. Kiaei, "A 10 MHz-bandwidth 2 mV-ripple PA-supply regulator for CDMA transmitters," in *IEEE Int. Solid-State Circuits Conf. Tech. Dig.*, Feb. 2008, pp. 448–449.
[15] J. Choi, D. Kim, D. Kang, and B. Kim, "A polar transmitter with CMOS programmable hysteretic-controlled hybrid switching supply modulator for multi-standard applications," *IEEE Trans. Microw. Theory Tech.*, vol. 57, no. 7, pp. 1675–1686, Jul. 2009.
[16] J. Choi, D. Kang, D. Kim, J. Park, B. Jin, and B. Kim, "Power amplifiers and transmitters for next generation mobile handset," *J. Semicond. Tech. Sci.*, vol. 9, no. 4, pp. 249–256, Dec. 2009.
[17] Y. Y. Woo, Y. Yang, and B. Kim, "Analysis and experiments for high efficiency class-F and inverse class-F power amplifiers," *IEEE Trans. Microw. Theory Tech.*, vol. 54, no. 5, pp. 1969–1974, May 2006.
[18] P. Colantonio, F. Giannini, G. Leuzzi, and E. Limiti, "On the class-F power amplifier design," *Int. J. RF Microw. Comput.-Aided Eng.*, vol. 9, no. 2, pp. 129–149, 1999.
[19] P. Wright, J. Lees, J. Benedikt, P. J. Tasker, and S. C. Cripps, "A methodology for realizing high efficiency class-J in a linear and broadband PA," *IEEE Trans. Microw. Theory Tech.*, vol. 57, no. 12, pp. 3196–3204, Dec. 2009.

[20] P. Butterworth, S. Gao, S. F. Ool, and A. Sambell, "High-efficiency class-F power amplifier with broadband performance," *Microw. Opt. Technol. Lett.*, vol. 44, no. 3, pp. 243–247, Feb. 2005.

[21] Y. Qin, S. Gao, P. Butterworth, E. Korolkiewicz, and A. Sambell, "Improved design technique of a broadband class-E power amplifier at 2 GHz," in *Proc. Eur. Microw. Conf.*, Oct. 2005, vol. 1, pp. 453–456.

[22] D. Kang, J. Choi, M. Jun, D. Kim, J. Park, B. Jin, D. Yu, K. Min, and B. Kim, "Broadband class-F power amplifiers for handset applications," in *Proc. 39th Eur. Microw. Conf.*, Sep. 2009, pp. 1547–1550.

[23] D. Kim, J. Choi, D. Kang, J. Choi, and B. Kim, "High efficiency and wideband ET PA with sweet spot tracking," in *Proc. IEEE Radio Freq. Integr. Circuits Symp.*, 2010, pp. 255–258.

[24] Y. Zhao, A. Metzger, P. Zampardi, M. Iwamoto, and P. Asbeck, "Linearity improvement of HBT-based Doherty power amplifiers based on a simple analytical model," *IEEE Trans. Microw. Theory Tech.*, vol. 54, no. 12, pp. 4479–4488, Dec. 2006.

[25] D. Kang, D. Yu, K. Min, K. Han, J. Choi, B. Jin, D. Kim, M. Jeon, and B. Kim, "A highly efficient and linear class-AB/F power amplifier for multi-mode operation," *IEEE Trans. Microw. Theory Tech.*, vol. 56, no. 1, pp. 77–87, Jan. 2008.

[26] D. M. Pozar, *Microwave Engineering*. Hoboken, NJ: Wiley, 2005.

Jooseung Kim received the B.S. degree in electrical engineering from the Pohang University of Science and Technology (POSTECH), Pohang, Korea, in 2010, and is currently working toward the Ph.D. degree in electrical engineering at POSTECH.

His research interests are CMOS RF circuits for wireless communications with a special focus on highly efficient and linear RF transmitter design.

Daehyun Kang received the B.S. degree in electronic and electrical engineering from Kyungpook National University, Daegu, Korea, in 2006, and is currently working toward the Ph.D. degree in electrical engineering at the Pohang University of Science and Technology (POSTECH), Pohang, Korea.

His main interests are RF circuits for wireless communications, especially highly efficient and linear RF transmitters and RF PA design.

Yunsung Cho received the B.S. degree in electrical engineering from Hanyang University, Ansan, Korea, in 2010, and is currently working toward the Ph.D. degree in electrical engineering at the Pohang University of Science and Technology (POSTECH), Pohang, Korea.

His main interests are RF circuits for wireless communications with a special focus on highly efficient and linear RF transmitters and RF PA design.

Dongsu Kim received the B.S. degree in electrical engineering from the Pohang University of Science and Technology (POSTECH), Pohang, Korea, in 2007, and is currently working toward the Ph.D. degree in electrical engineering at POSTECH.

His research interests are CMOS RF circuits for wireless communications, with a special focus on highly efficient and linear RF transmitter design.

Bumman Kim (M'78–SM'97–F'07) received the Ph.D. degree in electrical engineering from Carnegie.Mellon University, Pittsburgh, PA, in 1979.

From 1978 to 1981, he was engaged in fiber-optic network component research with GTE Laboratories Inc. In 1981, he joined the Central Research Laboratories, Texas Instruments Incorporated, where he was involved in development of GaAs power field-effect transistors (FETs) and monolithic microwave integrated circuits (MMICs). He has developed a large-signal model of a power FET, dual-gate FETs for gain control, high-power distributed amplifiers, and various millimeter-wave MMICs. In 1989, he joined the Pohang University of Science and Technology (POSTECH), Pohang, Gyungbuk, Korea, where he is currently a Namko Professor with the Department of Electrical Engineering, and Director of the Microwave Application Research Center, where he is involved in device and circuit technology for RF integrated circuits (RFICs). In 2001, he was a Visiting Professor of electrical engineering with the California Institute of Technology, Pasadena. He has authored over 200 technical papers.

Dr. Kim is a member of the Korean Academy of Science and Technology and the Academy of Engineering of Korea. He was an associate editor for the IEEE TRANSACTIONS ON MICROWAVE THEORY AND TECHNIQUES and a Distinguished Lecturer of the IEEE Microwave Theory and Techniques Society (IEEE MTT-S).

Jinsung Choi received the B.S. and Ph.D. degrees in electrical engineering from the Pohang University of Science and Technology (POSTECH), Pohang, Korea, in 2004 and in 2010, respectively.

He is currently with the Samsung Advanced Institute of Technology (SAIT), Yongin-si, Korea. His main research interests are analog/RF circuit design in ultra-deep submicrometer CMOS technology, mixed-mode signal-processing integrated-circuit design, and digitally assisted RF transceiver architectures.